Atmos. Chem. Phys. Discuss., 13, 8901–8937, 2013
www.atmos-chem-phys-discuss.net/13/8901/2013/
doi:10.5194/acpd-13-8901-2013

Atmospheric Chemistry and Physics Discussions

Global ozone–CO correlations from OMI and AIRS: constraints on tropospheric ozone sources

P. S. Kim[1], D. J. Jacob[1,2], X. Liu[3], J. X. Warner[4], K. Yang[5,6], and K. Chance[3]

[1]Harvard University, Department of Earth and Planetary Sciences, Cambridge, MA, USA
[2]Harvard University, School of Engineering and Applied Sciences, Cambridge, MA, USA
[3]Harvard–Smithsonian Center for Astrophysics, Cambridge, MA, USA
[4]University of Maryland, College Park, College of Computer, Mathematical and Natural Science, College Park, Maryland, USA
[5]University of Maryland, College Park, Department of Atmospheric and Oceanic Science, Maryland, USA
[6]NASA Goddard Space Flight Center, Greenbelt, MD, USA

Received: 7 March 2013 – Accepted: 15 March 2013 – Published: 3 April 2013

Correspondence to: P. S. Kim (kim68@fas.harvard.edu)

Published by Copernicus Publications on behalf of the European Geosciences Union.

Abstract

We present a global data set of free tropospheric ozone–CO correlations with $2^{\circ} \times 2.5^{\circ}$ spatial resolution from the Ozone Monitoring Instrument (OMI) and Atmospheric Infrared Sounder (AIRS) satellite instruments for each season of 2008. OMI and AIRS have near daily global coverage of ozone and CO respectively and observe coincident scenes with similar vertical sensitivities. The resulting ozone–CO correlations are highly statistically significant (positive or negative) in most regions of the world, and are less noisy than previous satellite-based studies that used sparser data. We interpret the observed ozone–CO correlations with the GEOS-Chem chemical transport model to infer constraints on ozone sources. Driving GEOS-Chem with different meteorological fields generally shows consistent ozone–CO correlation patterns, except in some tropical regions where the correlations are strongly sensitive to model transport error associated with deep convection. GEOS-Chem reproduces the general structure of the observed ozone–CO correlations and regression slopes (dO_3/dCO), although there are some large regional discrepancies. We examine the model sensitivity of dO_3/dCO to different ozone sources (combustion, biosphere, stratosphere, and lightning NO_x) by correlating the ozone change from that source to CO from the standard simulation. The model reproduces the observed positive dO_3/dCO in the extratropical Northern Hemisphere in spring–summer, driven by combustion sources. Stratospheric influence there is also associated with a positive dO_3/dCO because of the interweaving of stratospheric downwelling with continental outflow. The well-known ozone maximum over the tropical South Atlantic is associated with negative dO_3/dCO in the observations; this feature is reproduced in GEOS-Chem and supports a dominant contribution from lightning to the ozone maximum. A major model discrepancy is found over the Northeast Pacific in summer-fall where dO_3/dCO is positive in the observations but negative in the model, for all ozone sources. We suggest that this reflects a model overestimate of lightning at northern mid-latitudes combined with an underestimate of the East Asian CO source.

ACPD
13, 8901–8937, 2013

1 Introduction

Tropospheric ozone is produced by the photochemical oxidation of carbon monoxide (CO) and volatile organic compounds (VOCs) in the presence of nitrogen oxides ($NO_x \equiv NO + NO_2$). It is a potent greenhouse gas and harmful surface air pollutant, with implications for climate, human health, and agricultural productivity. Current global models can capture the observed large-scale spatial and seasonal patterns of ozone concentrations but there is large uncertainty in the driving factors, as reflected by the large differences between models in ozone production and loss rates (Wild, 2007; Wu et al., 2007) and in source contributions (Fiore et al., 2009). We present here a high-density global satellite database of ozone–CO correlations using data from the Ozone Monitoring Instrument (OMI; Levelt et al., 2006) and the Atmospheric Infrared Sounder (AIRS; Aumann et al., 2003), and explore its value for constraining our understanding of the factors controlling ozone.

Many studies have used ozone–CO correlations derived from in situ observations to constrain ozone sources and transport. CO is emitted from incomplete combustion and has an atmospheric lifetime of a few months against oxidation. Fishman and Seiler (1983) first used the sign of the ozone–CO correlation in aircraft observations to distinguish between ozone produced photochemically in the troposphere (positive) and transported down from the stratosphere (negative). Positive surface air correlations observed in aged pollution and biomass burning plumes have been used to infer ozone production efficiencies (OPEs) and continental export (Parrish et al., 1993; Chin et al., 1994; Hirsch et al., 1996; Mao and Talbot, 2004; Jaffe and Wigder, 2012). Negative correlations may result from ozone chemical loss and surface deposition (Cardenas et al., 1998; Parrish et al., 1998; Harris et al., 2000). Observations from aircraft and remote mountain sites show that ozone–CO correlations extend into the free troposphere and on intercontinental scales, although they then reflect mixing of air masses as well as chemistry (Andreae et al., 1994; Mauzerall et al., 1998; Zahn et al., 2002; Honrath et al., 2004; Hudman et al., 2007). Interleaving of stratospheric intrusions with polluted

ACPD
13, 8901–8937, 2013

continental outflow can complicate the fine-scale correlations in the free troposphere (Nowak et al., 2004; Price et al., 2004; Liang et al., 2007).

Coincident satellite observations providing global coverage of ozone and CO have become available over the past decade from the NASA A-Train constellation. The vertical resolution of satellite retrievals is typically limited to 1–2 pieces of information in the troposphere. Zhang et al. (2006) first demonstrated that ozone–CO correlations could be derived from Tropospheric Emission Spectrometer (TES) retrievals of the mid-troposphere (Beer et al., 2001). Hegarty et al. (2009, 2010) examined ozone–CO correlations from TES grouped by the predominant synoptic circulation patterns over North America, and found a well-defined positive relationship in continental export in spring–summer. Voulgarakis et al. (2011) used TES data from 2005–2008 to derive global ozone–CO correlation statistics for December–January and July–August, and compared to results from two global models. They concluded that a systematic underestimate of the TES-derived ozone–CO correlations by the UKCA model was likely caused by model transport errors.

All previous ozone–CO correlation analyses from space have used ozone and CO satellite data from the TES instrument. A drawback is the limited coverage of TES due to lack of cross-track scanning. Individual satellite retrievals have large random error, compromising correlation analyses unless large ensembles are considered. Correlation analyses using TES have had to aggregate the data over ~ 1000 km spatial domains and/or over several years. Even so, the random retrieval error is problematic when diagnosing ozone–CO correlations (Zhang et al., 2006).

In this work, we produce a new database of ozone–CO correlations from space using ozone retrievals from OMI and CO retrievals from AIRS. These two instruments aboard the NASA A-Train observe the same scenes with near-coincidence (< 15 min). They use different spectral bands (OMI in the UV, AIRS in the thermal IR) but their vertical sensitivities are similar. Both provide near-daily global coverage. This allows us to calculate robust statistical relationships between ozone and CO with much less error and finer spatiotemporal resolution than previous satellite studies. Here we present global

ACPD
13, 8901–8937, 2013

ozone–CO correlations for each season of 2008 on a $2^\circ \times 2.5^\circ$ grid, and we use the global GEOS-Chem chemical transport model (CTM) to interpret these correlations. A subsequent paper will examine interannual variability.

2 Data and methods

2.1 OMI

The OMI instrument is onboard the NASA Aura satellite with an equator crossing time of ~13:45 LT. It measures solar backscatter at 270–500 nm. The nadir footprint is $13 \times 24\,\mathrm{km}^2$, with near-daily global coverage from its 2600 km cross-track pushbroom scanner. We use the Level 2G product of PROFOZ ozone profile retrievals by Liu et al. (2010), with a few major modifications described below. This retrieval is based on the optimal estimation method of Rodgers (2000). It reports partial ozone columns for 24 layers extending from the surface to ~0.1 hPa. The retrieved vertical profile of partial ozone columns, described by the vector $\hat{\boldsymbol{x}}$, can be expressed as

$$\hat{\boldsymbol{x}} = \mathbf{A}\boldsymbol{x} + (\mathbf{I} - \mathbf{A})\boldsymbol{x}_\mathrm{a} + \epsilon \quad (1)$$

where $\mathbf{A}$ is the averaging kernel matrix, $\boldsymbol{x}$ is the true vertical profile, $\mathbf{I}$ is the identity matrix, $\boldsymbol{x}_\mathrm{a}$ is the a priori estimate, and ϵ is the retrieval error. The averaging kernel matrix represents the sensitivity of the retrieval to the true profile.

To speed up processing, the retrieval is done here at a nadir resolution of $52 \times 48\,\mathrm{km}^2$ by co-adding 4/8 OMI UV1 (270–310 nm)/UV2 (310–330 nm) pixels. A major change to the retrieval presented by Liu et al. (2010) is the constraint on measurement error. Liu et al. (2010) used OMI random-noise measurement error to constrain the retrievals. However, recent downward revision of this measurement error (Braak, 2010), together with further reduction of this error through co-adding, results in unrealistically small observational error specification (~0.035 % at 320 nm under tropical clear conditions) that causes spurious variability in the retrieval. This is most likely due to other unaccounted

ACPD
13, 8901–8937, 2013

measurement and forward modeling errors. Therefore a minimum measurement error of 0.2 % in the spectral region of 300–330 nm is imposed. In addition, Liu et al. (2010) used effective O_3 cross-sections and performed calculations at the OMI spectral grid resolution, which causes radiance errors up to 0.2–0.6 % at some wavelengths (with spectral position and magnitude errors varying with solar zenith angle). In the new algorithm, the radiative transfer calculation is done using VLIDORT (Spurr, 2006) as in Liu et al. (2010), but is now performed at selected wavelengths, interpolated to a fine grid of 0.05 nm using weighting functions, and is then convolved with OMI slit functions. This new scheme can reduce the radiance errors to typically less than 0.1 %.

The PROFOZ retrievals typically have 0.5–1.0 degrees of freedom for signal (DOFS), usually peaking at 700–500 hPa. We filter out poor retrievals by requiring that the average and root mean square (RMS) fitting residuals provided by the retrieval for the UV-2 channel be less than 3 % of the measurement error, and we also exclude data poleward of 60° due to high solar zenith angles.

The a priori estimate for the PROFOZ retrieval uses the McPeters et al. (2007) ozone profile climatology, which depends on calendar month and latitude. This adds variability to the retrieved profiles that is not actually measured. We remove this variability as in Zhang et al. (2006) by reprocessing the OMI retrievals to use a fixed a priori profile everywhere, which we choose as the mean annual McPeters et al. (2007) profile for 30° S–30° N.

Intercomparison of the OMI PROFOZ and TES ozone retrievals by Zhang et al. (2010) shows that the two exhibit similar geographic and seasonal variability with differences generally within ±10 ppbv. Validation of the OMI PROFOZ retrieval with ozonesonde profiles shows a global mean positive bias of 2.8 ppb in the troposphere (Zhang et al., 2010), which we subtract from the retrieved values.

2.2 AIRS

The AIRS instrument is onboard the NASA Aqua satellite with an equator crossing time of ~ 13:30 LT. AIRS retrieves CO by observing thermal emission around the 4.7 μm

ACPD
13, 8901–8937, 2013

vibrational fundamental band. We use the Level 2 CO profiles from the version 5 (v5) AIRS retrieval (available for download through ftp://airspar1u.ecs.nasa.gov). A detailed description of the retrieval algorithm is available in Susskind et al. (2003). We use the Support retrieval product, which includes higher resolution profiles than the Standard product, reporting CO partial columns on 100 pressure levels between 1100 and 0.016 hPa. AIRS CO retrievals typically have ∼0.8 DOFS with sensitivity generally peaking between 600 and 300 hPa (Warner et al., 2007). The AIRS a priori is a fixed vertical profile from Deeter et al. (2003) up to 10.25 hPa and from the Air Force Geophysics Laboratory (AFGL) standard atmosphere profile above.

Validation of the AIRS v5 retrieval with aircraft vertical profiles shows a positive bias of 6–10 % in the Northern Hemisphere (McMillan et al., 2011) with a larger positive bias in the Southern Hemisphere (Yurganov et al., 2008, 2010; Warner et al., 2010). To correct for this bias we scale AIRS profiles down by 10 %. We remove retrievals that do not have quality flag QA = 0 provided in the retrieval product as well as any profiles with surface temperature reported as less than 250 K. For consistency with OMI, we limit our analysis to the daytime retrievals.

2.3 GEOS-Chem

We use the GEOS-Chem global CTM (version 9-01-02, http://geos-chem.org), originally described by Bey at al. (2001) and Park et al. (2004), to interpret the observed satellite ozone–CO relationships. GEOS-Chem is driven by Goddard Earth Observing System (GEOS-5) assimilated meteorological data from the NASA Global Modeling and Assimilation Office (GMAO). The GEOS-5 meteorological data have a native horizontal resolution of $0.5^\circ \times 0.67^\circ$ with 72 vertical pressure levels and 6 h temporal frequency (3 h for surface variables and mixing depths). We degrade the horizontal resolution to $2^\circ \times 2.5^\circ$ for input to GEOS-Chem. The model results presented here are for 2008 following a 1 yr initialization.

Global anthropogenic emissions of CO, NO_x, and SO_2 are from the EDGAR 3.2 inventory (Olivier and Berdowski, 2001) while anthropogenic non-methane VOCs are

ACPD
13, 8901–8937, 2013

from the RETRO monthly global inventory for 2000 (van het Bolscher et al., 2008). Regional overwrites are used where available. These include the US EPA NEI inventory for 2005, Asian emissions from Zhang et al. (2009), the EMEP inventory for Europe (Vestreng and Klein, 2002), the CAC emission inventory for Canada, and the BRAVO emission inventory for Mexico (Kuhns et al., 2005). Global biofuel emissions are from Yevich and Logan (2003). Biomass burning emissions are from the Global Fire Emission Database version 3 (GFED3) inventory with monthly resolution (Giglio et al., 2010; van der Werf et al., 2010). Biogenic VOC emissions are from the Model of Emissions of Gases and Aerosols from Nature (MEGAN) inventory of Guenther et al. (2006). The present simulation also includes conversion of HO_2 to H_2O in aerosol particles (Mao et al., 2013).

Lightning NO_x emissions are constrained by an OTD/LIS climatology of lightning flash observations from satellites as described by Sauvage et al. (2007) and Murray et al. (2012), with timing and vertical distribution determined by GEOS-Chem deep convection. The global lightning NO_x source is $6\,Tg\,N\,a^{-1}$ (Martin et al., 2007) with higher NO_x yield per flash at northern mid-latitudes compared to the tropics (Hudman et al., 2007).

Vertical profiles of ozone and CO in the stratosphere are simulated in GEOS-Chem using GEOS-5 transport, as in the troposphere, but with climatological production and loss rate constants. Production and loss rate constants for ozone in the stratosphere are computed locally with the Linoz algorithm of McLinden et al. (2000), while those for CO are specified on a monthly basis from the 2-D model of Schneider et al. (1999).

Previous evaluations of the ozone and CO simulations with OMI and AIRS by Zhang et al. (2010) and Kopacz et al. (2010) showed that GEOS-Chem is in general consistent with observations. However, several regional biases were apparent in these studies. In particular, the ozone simulation of Zhang et al. (2010) underestimated ozone in the tropics while overestimating ozone in the northern subtropics and southern mid-latitudes. We will discuss these biases in the context of the present simulation below.

ACPD
13, 8901–8937, 2013

2.4 Correlation statistics

We average the individual OMI ozone and AIRS CO profile retrievals over a 2° × 2.5° horizontal grid, based on the center of the satellite footprint, for each day of 2008. We focus on the 700–400 hPa columns, where both instruments have maximum sensitivity. These are computed by adding the corresponding partial columns in the retrievals, with linear interpolation as necessary. For clarity of presentation, we convert the partial columns to the corresponding column mixing ratios. We compute the 700–400 hPa DOFS by adding the corresponding elements of the diagonal of the averaging kernel matrix and remove scenes with DOFS less than 0.1.

We compute seasonal ozone–CO correlation statistics, specifically the correlation coefficient (r) and reduced-major-axis (RMA) regression slope (dO_3/dCO), for the 3-month time series (DJF, MAM, JJA, SON) of the ozone and CO mixing ratios for each grid square. The magnitude of the RMA slope is independent of the magnitude of the correlation coefficient and comparisons to previous studies using ordinary least squares (OLS) regression slopes can be made by dividing the RMA slopes reported here by the absolute value of the correlation coefficient (Isobe et al., 1990).

For comparison to the satellite data, we archive GEOS-Chem daily output at the local satellite overpass time and regrid it vertically to the instrument retrieval levels. Since GEOS-Chem has little predictive capability in the stratosphere due to the use of climatological chemical rates, we replace the simulated profiles above the tropopause with the observed profiles as in Zhang et al. (2006). The simulated ozone and CO profiles are then smoothed with the instrument averaging kernels to account for the measurement sensitivity. The ozone–CO statistics from GEOS-Chem are calculated using the same methodology as the satellite data described above.

Random noise in individual ozone and CO profile retrievals degrades the ozone–CO correlations but this can be greatly reduced by averaging (central limit theorem). The high density of OMI and AIRS observations is of considerable advantage for this purpose. After data filtering, there are typically 10–30 OMI and AIRS profiles binned daily

ACPD
13, 8901–8937, 2013

in each 2° × 2.5° grid square where data is available, with more profiles at lower latitudes. Tests applying random retrieval error to the GEOS-Chem profiles, as in Zhang et al. (2006), indicate little effect of retrieval noise on the simulated ozone–CO correlations from OMI and AIRS. This is in contrast to the TES results of Zhang et al. (2006) and Voulgarakis et al. (2011) where the correlations were found to be significantly degraded by that noise.

3 Global ozone–CO correlation patterns

Figure 1a, b shows global maps of the 2008 seasonal mean mixing ratios for AIRS CO and OMI ozone at 700–400 hPa. CO is highest over and downwind of combustion source regions (fossil fuel, seasonal fires). The spring maximum is primarily driven by photochemical loss of CO from reaction with OH. Ozone features the well-known spring–summer maximum in the northern extratropics (Monks, 2000) and minimum over the tropics except for biomass burning regions and the South Atlantic (Martin et al., 2002). Ozone at southern mid-latitudes peaks in winter–spring, reflecting a combination of stratospheric and biomass burning influences (Zhang et al., 2010).

Comparison of Fig. 1 to the corresponding seasonal mean distributions for ozone and CO simulated by GEOS-Chem (Fig. S1a, b in the Supplement) shows that the model generally reproduces the large-scale patterns and seasonal cycles of both species. In contrast to the results of Zhang et al. (2010), we find an underestimate in ozone relative to OMI in the northern mid-latitudes, likely reflecting the conversion of HO_2 to H_2O in aerosol particles in the present work from Mao et al. (2013).

Figure 2a shows the observed seasonal ozone–CO correlation coefficients from OMI and AIRS and compares them to the corresponding GEOS-Chem values. The correlations are in general highly statistically significant. Strong positive correlations are observed in all seasons in the northern subtropics, particularly downwind of the continents. The strongest correlations are in MAM and JJA, with r exceeding 0.8 over the western Pacific. GEOS-Chem shows moderate skill in capturing the magnitude

ACPD
13, 8901–8937, 2013

of these positive correlations and their seasonal cycle, performing particularly well in MAM. The most prominent discrepancies in the northern extratropics are over Eurasia and the Northeast Pacific in JJA and SON where model correlations are negative. We will examine the cause of these discrepancies in the next section.

Observed correlations in the tropics are weak in DJF but generally strong in other seasons, with positive or negative values depending on region. Positive correlations in the northern tropics appear to be an extension of the subtropics. The strongest negative correlation in the tropics is over the Caribbean in JJA, with r exceeding −0.7. GEOS-Chem captures these large negative values over the Caribbean, but erroneously shows the negative correlations extending east across the tropical Atlantic and North Africa in all seasons.

Strong positive correlations are observed over the southern tropical oceans in MAM, and expand into a near zonal band from 0°–30° S in JJA and SON. GEOS-Chem is unable to fully reproduce this zonal structure. In DJF, strong negative r values are observed off the coast of Peru and Indonesia. GEOS-Chem captures the negative correlations near Peru, but overestimates their spatial extent and magnitude. In addition, the model simulates r values of the wrong sign over Indonesia in all seasons except MAM. With the exception of JJA, GEOS-Chem incorrectly simulates strong negative correlations over much of South America.

The observed OMI/AIRS correlations reported here are broadly consistent with previous TES results for July 2005 (Zhang et al., 2006), spring seasonal composites for the North Atlantic (Hegarty et al., 2009), and the four-year global July–August results (Voulgarakis et al., 2011). The higher data density from OMI/AIRS provides finer-scale information. We find regional discrepancies with the Voulgarakis et al. (2011) TES analysis for December–January, for example in the sign of r over Indonesia. This may reflect interannual variability or actual inconsistency between the TES and OMI/AIRS product. We will address this issue in future work.

The RMA regression slopes for OMI/AIRS and GEOS-Chem are shown in Fig. 2b. The patterns are similar to those of the correlation coefficients (RMA slopes must have

ACPD
13, 8901–8937, 2013

the same sign but are not otherwise related to the *r* values). In the next section, we will interpret the RMA slopes in terms of the information that they contain for the sources of ozone.

4 Interpretation of the ozone–CO relationship

Ozone–CO correlations reflect a combination of transport and chemistry. In pollution outflow mixing with a relatively clean background, the ozone–CO relationship gives a measure of the OPE for that pollution source region (Parrish et al., 1993; Hirsch et al., 1996). In stratospheric intrusions mixing with tropospheric air, the ozone–CO relationship reveals the stratospheric influence on ozone (Fishman and Seiler, 1983). In general, however, the relative contributions of transport and chemistry in driving the ozone–CO relationship are not obvious, especially in the free troposphere where the chemistry is relatively slow and pollution enhancements are relatively weak. Previous studies for the free troposphere have highlighted how interpretation of ozone–CO correlations is complicated by mixing of combustion plumes with variable background (Mauzerall et al., 1998) or by interleaving of stratospheric intrusions with polluted continental outflow (Nowak et al., 2004; Price et al., 2004; Liang et al., 2007). These complications motivate the use of a CTM to interpret the observed ozone–CO relationships.

Two previous studies have used CTMs to interpret observed satellite-based ozone–CO relationships. Zhang et al. (2008) found positive ozone–CO *r* values in two transpacific pollution events in both the TES retrievals and GEOS-Chem. They interpreted the observed correlations as indicative of Asian pollution influence on ozone, since the correlation disappeared in the model in a sensitivity simulation without Asian emissions. Voulgarakis et al. (2011) conducted sensitivity simulations with perturbed emissions in the G-PUCCINI and UKCA models to examine the importance of different sources in driving the global correlation patterns. They found that emissions were important for changing the magnitude of *r* downwind of source regions, with biomass burning in the tropics capable of changing the sign.

ACPD
13, 8901–8937, 2013

Here we use the GEOS-Chem CTM to interpret the OMI-AIRS ozone–CO correlations presented in Fig. 2. Our aim is to use the observed correlations as constraints on the model representation of ozone sources. This can be compromised if the simulated correlations are highly sensitive to model transport error. In that case, comparison to observed correlations would mainly serve as a convoluted test of model transport and be of little benefit. Thus we first examine the sensitivity of the ozone–CO correlations in GEOS-Chem to model transport error, diagnose the features that appear to be robust against this transport error, and then conduct a more focused examination of the sensitivity to ozone sources for regions of particular interest.

4.1 Sensitivity to model transport error

We examined the impact of model transport errors on the ozone–CO relationship simulated with GEOS-Chem by comparing the standard simulation driven by GEOS-5 meteorological data to a simulation driven by the previous-generation GEOS-4 meteorological data for the same year. Here we used 2006, for which both GEOS-5 and GEOS-4 data are available. GEOS-5 and GEOS-4 are very different in terms of both model physics (they use different general circulation models) and data assimilated. Previous studies have compared GEOS-5 and GEOS-4 simulations of CO (Liu et al., 2010) and CO_2 (Feng et al., 2011; Parazoo et al., 2012) and shown large differences reflecting the convective parameterizations.

Figure 3 shows ozone–CO correlations in JJA 2006 from OMI/AIRS, GEOS-Chem driven by GEOS-4, and GEOS-Chem driven by GEOS-5. The OMI/AIRS JJA correlations for 2006 (El Niño) are similar to the 2008 (La Niña) results shown in Fig. 2a, with slight differences over the United States and Southeast Asia. We find that the ozone–CO correlations simulated by GEOS-Chem using GEOS-5 and GEOS-4 meteorological fields generally show similar spatial patterns. The main differences are in the tropics, where GEOS-4 tends to simulate weaker negative correlations than GEOS-5. Over the Caribbean, this leads to an underestimate of the observed r values in GEOS-4 associated with a high bias in both ozone and CO; insufficient detrainment of clean

ACPD
13, 8901–8937, 2013

maritime air in the mid-troposphere appears to be responsible. In contrast, the GEOS-4 simulation is in better agreement with the observations than GEOS-5 off the west coast of northern Africa. This is attributed to errors in vertical mixing in GEOS-5 leading to a low bias in ozone and a high bias in CO.

Overall, we conclude that model transport errors can have significant regional impacts on simulated ozone–CO correlations. In some areas such as the Equatorial West Pacific, this completely compromises the ability to interpret dO_3/dCO in terms of ozone sources. In most regions, however, the general correlation patterns are sufficiently robust against model transport errors (at least for GEOS-5 vs. GEOS-4) that we can investigate them further to diagnose contributions from ozone sources.

4.2 Sensitivity to ozone sources

We now examine here whether the observed ozone–CO relationships can be used to place constraints on combustion (NO_x, CO, VOCs), biogenic (VOCs), lightning (NO_x), and stratospheric sources of ozone. All four are considered to be major sources of ozone, but their relative importance in different regions of the troposphere is uncertain (Stevenson et al., 2006; Wu et al., 2007; Terao et al., 2008; Baray et al., 2012). Starting from the standard GEOS-Chem simulation described in Sect. 2.3 and with results shown in Figs. S1 and 2, our approach is to conduct sensitivity simulations with individual sources shut off. Here we aggregate fossil fuels and biomass burning in the combustion source, with the understanding that the latter will mainly affect the tropics.

Zhang et al. (2006) and Voulgarakis et al. (2011) previously diagnosed the influence of individual sources on the ozone–CO relationship as the change in the ozone–CO correlation or slope (dO_3/dCO) between their standard CTM simulation and a sensitivity simulation with that source shut off. However, this does not provide a proper measure of the influence of the source on ozone because the ozone–CO relationship is then affected by changes in both ozone and CO. A more appropriate approach is to correlate CO from the standard simulation with the ozone difference between the standard and sensitivity simulations. Chin et al. (1994) previously used this approach to interpret

ACPD
13, 8901–8937, 2013

ozone–CO relationships from eastern North American surface sites in terms of ozone production.

We illustrate our approach in Fig. 4, which shows the simulated ozone–CO relationships at 700–400 hPa for a 2° × 2.5° grid square in JJA in the western North Atlantic (38° N, 70° W) receiving polluted continental outflow from North America (Zhang et al. (2006) had previously examined the ozone–CO relationships observed from TES and aircraft for the same region). In the left panel of Fig. 4, ozone from the standard simulation is shown in black and ozone from a simulation without combustion sources is shown in red, both plotted against CO from the standard simulation. The ozone–CO slope and 95 % confidence interval calculated using nonparametric bootstrapping for the standard simulation are shown inset. We see that the ozone–CO correlation disappears without combustion sources, indicating that it provides a test of combustion influence. This is quantified in the right panel by plotting the ozone difference ΔO_3 between the standard and no combustion simulations against CO from the standard simulation. We find a strong positive slope $d\Delta O_3/dCO$ that can explain dO_3/dCO from the standard simulation to within the bootstrap errors in the linear regression.

Global maps of $d\Delta O_3/dCO$ for different ozone sources and seasons are presented in the Supplement and can be used to interpret the dO_3/dCO slopes in Fig. 2b. Here we focus our discussion on three illustrative regions of particular interest, outlined in white in Fig. 2b: (1) the North Atlantic in JJA, where US pollution outflow is known to take place and has been previously diagnosed from observed ozone–CO correlations; (2) the South Atlantic in DJF, where different explanations have been proposed for the origin of the observed ozone maximum; and (3) the Northeast Pacific in SON, where significant intercontinental transport of Asian pollution is expected. As shown in Fig. 2b, GEOS-Chem reproduces the observed dO_3/dCO from OMI/AIRS for (1) and (2) but fails for (3).

Figure 5 shows the observed and simulated dO_3/dCO for the three above regions along with $d\Delta O_3/dCO$ calculated for simulations without combustion, biogenic, lightning NO_x, and stratospheric ozone sources for 2008. The statistics are calculated by

ACPD
13, 8901–8937, 2013

aggregating all of the daily average ozone and CO data contained within the region boundaries. We also include in Fig. 5 the observed dO_3/dCO for 2006, along with model values for that year using both GEOS-5 and GEOS-4 meteorology. These allow us to examine interannual variability and the effect of transport errors as discussed above. Slope bounds in Fig. 5 represent the mean variance, which is computed from the variance of all bootstrap slope realizations for each individual grid within the region boundaries.

4.2.1 North Atlantic in JJA

The observed ozone–CO relationship at northern mid-latitudes shows a consistent positive correlation in continental outflow. Here we focus on the North Atlantic (Fig. 5a) but results are similar for the NW Pacific. The GEOS-Chem dO_3/dCO matches the observed slope of 0.51 ± 0.06 for 2008. The observed slopes show little difference between 2006 (0.56 ± 0.08) and 2008. The GEOS-Chem results using GEOS-5 and GEOS-4 in 2006 are consistent, suggesting that the ozone–CO relationship is robust against errors in transport.

From the $d\Delta O_3/dCO$ values in Fig. 5a we see that the O_3–CO correlation over the North Atlantic in JJA reflects a major contribution from combustion sources. Surface observations over the eastern US in summer typically show a dO_3/dCO value of 0.3–0.5, with higher values in more recent studies reflecting a decrease in CO emissions (Chin et al., 1994; Hirsch et al., 1996; Mao and Talbot, 2004; Hudman et al., 2008, 2009). We find in our sensitivity simulation that $d\Delta O_3/dCO$ from combustion sources decreases from west to east across the North Atlantic while dO_3/dCO remains roughly constant, suggesting little sustained photochemical production following lifting of the surface air to the free troposphere. The observed and simulated dO_3/dCO fall within the range of slopes observed by Honrath et al. (2004) at a mountaintop site in the Azores for 2001 and 2003.

Air mixing down from the stratosphere makes a small contribution to the ozone–CO regression slope, as shown in Fig. 5a. A remarkable result is that this effect is positive,

ACPD
13, 8901–8937, 2013

whereas stratospheric influence is commonly thought to be associated with a negative ozone–CO correlation (Fishman and Seiler, 1983). As shown by Cooper et al. (2002), stratospheric influence over the western North Atlantic is associated with the dry air stream (DA) of mid-latitudes cyclones, mixing with the warm conveyor belt (WCB) that lifts continental pollution to the free troposphere. This would lead to positive correlation of pollution and stratospheric influences when smoothed vertically over the averaging kernel of the satellite observations. A number of studies have shown ozone pollution plumes over the northern mid-latitude oceans to be interweaved with stratospheric influence (Nowak et al., 2004; Price et al., 2004; Liang et al., 2007).

Lightning NO_x has a large negative influence on dO_3/dCO over the North Atlantic, comparable in magnitude to the positive influence from combustion sources (Fig. 5a). Lightning NO_x produces both ozone and OH with high efficiency (Labrador et al., 2004), and OH oxidizes CO, thus leading in general to a negative $d\Delta O_3/dCO$ effect.

4.2.2 South Atlantic in DJF

Tropical tropospheric ozone shows a persistent maximum over the South Atlantic associated with strong subsidence (Thompson et al., 2000). The DJF ozone maximum is clearly seen by OMI (Fig. 1b) and is well reproduced by GEOS-Chem (Fig. S1b). The sources contributing to this maximum are not well understood. Different studies have argued for major contributions from combustion sources, including biomass burning in Africa (Thompson et al., 1996; Jourdain et al., 2007) and long-range transport of pollution (Chatfield et al., 2004), lightning NO_x (Martin et al., 2002; Sauvage et al., 2007), and intrusions of northern hemispheric air (Waugh and Polvani, 2000; Martin et al., 2002).

The statistical results in Fig. 5b show that the observed regression slope for the region is negative with a value of -0.54 ± 0.25. Good consistency is found between GEOS-Chem (either GEOS-5 or GEOS-4) and observations, and between 2006 and 2008.

ACPD
13, 8901–8937, 2013

We find that the ozone–CO relationship in the region is dominated by negative $d\Delta O_3/dCO$ contributions from lightning NO_x emissions. This implies that the ozone variability in the region is driven by lightning as suggested previously by Sauvage et al. (2007). The negative ozone–CO correlation associated with the lightning NO_x source reflects ozone production in the upper troposphere followed by strong subsidence of this photochemically aged air over the South Atlantic (Jacob et al., 1996; Martin et al., 2002). The $d\Delta O_3/dCO$ values in Fig. 5b suggest that stratospheric and combustion sources, including biomass burning, make little contribution to the ozone maximum over the South Atlantic.

4.2.3 Northeast Pacific in SON

The dO_3/dCO values derived from OMI and AIRS are positive in all seasons over the northeastern Pacific poleward of 20° N (Fig. 2b). GEOS-Chem reproduces this in DJF and MAM, but has negative slopes in JJA that extend across the entire eastern North Pacific by SON. The SON discrepancy is summarized in Fig. 5c. A slope of 0.75 ± 0.08 is observed in both 2006 and 2008, but GEOS-Chem simulates a negative slope using either GEOS-5 or GEOS-4 meteorology. The consistency between GEOS-5 and GEOS-4 suggests that an error in sources is responsible for the poor simulation.

The model shows negative $d\Delta O_3/dCO$ for all ozone sources including from combustion (Fig. 5c). This is because air masses over the Northeast Pacific are very remote from sources, having been transported across the Pacific and subsided slowly around the Pacific High. Ozone is produced efficiently in the subsiding air masses (Hudman et al., 2004; Zhang et al., 2008) while CO is oxidized. We find that GEOS-Chem over the region underestimates both ozone (mean difference of 1.9 ppb) and CO (8.0 ppb) compared to OMI and AIRS. Figure 5c shows that lightning is the principal driver of the negative dO_3/dCO values in GEOS-Chem.

Even in the absence of lightning influence, however, we see from Fig. 5c that GEOS-Chem would still produce negative dO_3/dCO values over the Northeast Pacific. This may reflect a model underestimate of CO emissions from East Asia, as supported by

ACPD
13, 8901–8937, 2013

the underestimate of AIRS CO mixing ratios (compare Figs. 1a and S1a) and by the work of Kopacz et al. (2010) who found from an inverse analysis using AIRS CO data that GEOS-Chem underestimates CO sources in China by up to a factor of two in SON. Such a bias in CO emissions could cause the $d\Delta O_3/dCO$ values from Asian pollution over the Northeast Pacific to flip from positive to negative.

5 Conclusions

Ozone–CO correlations provide a valuable constraint to test models of tropospheric ozone but have hitherto been limited to in-situ measurements and sparse satellite observations. By using satellite instruments with near-daily global coverage of the same scenes, OMI for ozone and AIRS for CO, we constructed a global data set of ozone–CO correlations in the free troposphere on a $2^\circ \times 2.5^\circ$ grid with seasonal resolution and for individual years. The high data density avoids the degradation of the correlations by instrument noise that was a problem in previous satellite studies. The correlation coefficients r are highly significant, showing strong positive values in continental outflow in the northern extratropics. The tropics and Southern Hemisphere show seasonally varying patterns of positive and negative correlations.

We interpreted the satellite-derived ozone–CO correlations with the GEOS-Chem chemical transport model to explore the constraints that they place on the model sources of ozone. By driving the model with different meteorological fields for the same year, we diagnosed the effect of model transport error on the correlations. This effect is large in some regions of the tropics, where the ozone–CO correlations are then of little value as a test of ozone sources. In general, however, we find that correlation patterns are consistent for different meteorological fields as well as different years, and can therefore be used as a test of ozone sources.

We tested the model sensitivity of the ozone–CO regression slope, dO_3/dCO, to different sources by conducting a series of sensitivity simulations with individual sources shut off (combustion, biosphere, stratosphere, lightning NO_x). From these we

ACPD
13, 8901–8937, 2013

calculated the source influence, $d\Delta O_3/dCO$, by correlating the ozone change from each source with CO from the standard simulation. The results provide global information on the sources responsible for the ozone–CO correlations in the model, thus enabling interpretation of comparisons of simulated and observed dO_3/dCO. We focused our discussion on three regions of particular interest.

The northern extratropics show strong positive dO_3/dCO in spring–summer that is driven by combustion sources and provides a test of the model simulation of continental outflow and intercontinental transport of ozone pollution. Remarkably, we find in that region that stratospheric influence (although weak) is also associated with a positive $d\Delta O_3/dCO$ value, reflecting its interweaving with pollution in continental outflow.

The well-known tropical ozone maximum over the South Atlantic is found to have a strongly negative dO_3/dCO, consistent for different years and meteorological data sets. GEOS-Chem reproduces this observation and attributes it to the strong contribution of lightning to the ozone maximum. Previous model studies that focused solely on simulating ozone had reached a range of conclusions as to the origin of the South Atlantic maximum, but the independent information from the ozone–CO correlations provides evidence of a dominant lightning source.

The Northeast Pacific is a region of particular interest for transpacific ozone pollution. Here we find that the GEOS-Chem fails to reproduce the observed ozone–CO correlation in summer–fall, yielding negative dO_3/dCO values when the observations show positive values. Remarkably, all ozone sources in the model yield negative $d\Delta O_3/dCO$ values in that region. This reflects the remote subsiding environment of the northeastern Pacific, where ozone is produced while CO is oxidized as air masses subside slowly around the Pacific High. Further analysis combined with independent evidence suggests that correcting this model bias would require both a reduction in the lightning source at northern mid-latitudes and an increase in CO emissions in East Asia.

We have shown in this paper that the combination of OMI ozone and AIRS CO provides a robust global data set of ozone–CO correlations in the free troposphere, and that these correlations provide a powerful tool for testing ozone sources in global

ACPD
13, 8901–8937, 2013

models. In future work we will exploit this data set further to examine interannual variability in ozone–CO correlations and the implications for our understanding of ozone sources.

Supplementary material related to this article is available online at: http://www.atmos-chem-phys-discuss.net/13/8901/2013/acpd-13-8901-2013-supplement.pdf.

Acknowledgements. This work was funded by the NASA Aura Program and in part by the Department of Energy Office of Science Graduate Fellowship Program (DOE SCGF), made possible in part by the American Recovery and Reinvestment Act of 2009, administered by ORISE-ORAU under contract no. DE-AC05-06OR23100.

References

Andreae, M. O., Anderson, B. E., Blake, D. R., Bradshaw, J. D., Collins, J. E., Gregory, G. L., Sachse, G. W., and Shipham, M. C.: Influence of plumes from biomass burning on atmospheric chemistry over the equatorial and tropical South Atlantic during CITE 3, J. Geophys. Res., 99, 12793–12808, doi:10.1029/94JD00263, 1994.

Aumann, H. H., Chahine, M. T., Gautier, C., Goldberg, M. D., Kalnay, E., McMillin, K. M., Revercomb, H., Rosenkranz, P. W., Smith, W. L., Staelin, D. H., Strow, L. L., and Susskind, J.: AIRS/AMSU/HSB on the Aqua mission: design, science objectives, data products, and processing systems, IEEE T. Geosci. Remote, 41, 253–264, doi:10.1109/TGRS.2002.808356, 2003.

Baray, J.-L., Duflot, V., Posny, F., Cammas, J.-P., Thompson, A. M., Gabarrot, F., Bonne, J.-L., and Zeng, G.: One year ozonesonde measurements at Kerguelen Island (49.2° S, 70.1° E): influence of stratosphere-to-troposphere exchange and long-range transport of biomass burning plumes, J. Geophys. Res., 117, D06305, doi:10.1029/2011JD016717, 2012.

ACPD
13, 8901–8937, 2013

Beer, R., Glavich, T. A., and Rider, D. M.: Tropospheric emission spectrometer for the Earth Observing System's Aura satellites, Appl. Optics, 40, 2356–2367, doi:10.1364/AO.40.002356, 2001.

Bey, I., Jacob, D. J., Yantosca, R. M., Logan, J. A., Field, B., Fiore, A. M., Li, Q., Liu, H., Mickley, L. J., and Schultz, M.: Global modeling of tropospheric chemistry with assimilated meteorology: model description and evaluation, J. Geophys. Res., 106, 23073–23096, doi:10.1029/2001JD000807, 2001.

Braak, R.: Bug fix for GDPS measurement noise calculation algorithm, KNMI, Technical Note TN-OMIE-KNMI-935, 2010.

Cardenas, L. M., Austin, J. F., Burgess, R. A., Clemitshaw, K. C., Dorling, S., Penkett, S. A., and Harrison, R. M.: Correlations between CO, NO_y, O_3, and non-methane hydrocarbons and their relationships with meteorology during winter 1993 on the north Norfolk coast, UK, Atmos. Environ., 32, 3339–3351, doi:10.1016/S1352-2310(97)00445-7, 1998.

Chatfield, R. B., Guan, H., Thompson, A. M., and Witte, J. C.: Convective lofting links Indian Ocean air pollution to paradoxical South Atlantic ozone maxima, Geophys. Res. Lett., 31, L06103, doi:10.1029/2003GL018866, 2004.

Chin, M., Jacob, D. J., Munger, J. W., Parrish, D. D., and Doddridge, B. G.: Relationship of ozone and carbon monoxide over North America and its implication for ozone production and transport, J. Geophys. Res., 99, 14565–14573, doi:10.1029/94JD00907, 1994.

Cooper, O. R., Moody, J. L., Parrish, D. D., Trainer, M., Ryerson, T. B., Holloway, J. S., Hubler, G., Fehsenfeld, F. C., and Evans, M. J.: Trace gas composition of midlatitude cyclones over the western North Atlantic Ocean: a conceptual model, J. Geophys. Res., 107, D04056, doi:10.1029/2001JD000901, 2002.

Deeter, M. N., Emmons, L. K., Francis, G. L., Edwards, D. P., Gille, J. C., Warner, J. X., Khattatov, B., Ziskin, D., Lamarque, J.-F., Ho, S.-P., Yudin, V., Attie, J.-L., Packman, D., Chen, J., Mao, D., Drummond, J. R.: Operational carbon monoxide retrieval algorithm and selected results for the MOPITT instrument, J. Geophys. Res., 108, 4399, doi:10.1029/2002JD003186, 2003.

Feng, L., Palmer, P. I., Yang, Y., Yantosca, R. M., Kawa, S. R., Paris, J.-D., Matsueda, H., and Machida, T.: Evaluating a 3-D transport model of atmospheric CO_2 using ground-based, aircraft, and space-borne data, Atmos. Chem. Phys., 11, 2789–2803, doi:10.5194/acp-11-2789-2011, 2011.

ACPD
13, 8901–8937, 2013

Fiore, A. M., Dentener, F. J., Wild, O., Cuvelier, C., Schultz, M. G., Hess, P., Textor, C., Schulz, M., Doherty, R. M., Horowitz, L. W., MacKenzie, I. A., Sanderson, M. G., Shindell, D. T., Stevenson, D. S., Szopa, S., Van Dingenen, R., Zeng, G., Atherton, C., Bergmann, D., Bey, I., Carmichael, G., Collins, W. J., Duncan, B. N., Faluvegi, G., Folberth, G., Gauss, M., Gong, S., Hauglustaine, D., Holloway, T., Isaksen, I. S. A., Jacob, D. J., Jonson, J. E., Kaminski, J. W., Keating, T. J., Lupu, A., Marmer, E., Montanaro, V., Park, R. J., Pitari, G., Pringle, K. J., Pyle, J. A., Schroeder, S., Vivanco, M. G., Wind, P., Wojcik, G., Wu, S., and Zuber, A.: Multimodel estimates of intercontinental source-receptor relationships for ozone pollution, J. Geophys. Res., 114, D04301, doi:10.1029/2008JD010816, 2009.

Fishman, J. and Seiler, W.: Correlative nature of ozone and carbon monoxide in the troposphere: implications for the tropospheric ozone budget, J. Geophys. Res., 88, 3662–3670, doi:10.1029/JC088iC06p03662, 1983.

Giglio, L., Randerson, J. T., van der Werf, G. R., Kasibhatla, P. S., Collatz, G. J., Morton, D. C., and DeFries, R. S.: Assessing variability and long-term trends in burned area by merging multiple satellite fire products, Biogeosciences, 7, 1171–1186, doi:10.5194/bg-7-1171-2010, 2010.

Guenther, A., Karl, T., Harley, P., Wiedinmyer, C., Palmer, P. I., and Geron, C.: Estimates of global terrestrial isoprene emissions using MEGAN (Model of Emissions of Gases and Aerosols from Nature), Atmos. Chem. Phys., 6, 3181–3210, doi:10.5194/acp-6-3181-2006, 2006.

Harris, J. M., Dlugokencky, E. J., Oltmans, S. J., Tans, P. P., Conway, T. J., Novelli, P. C., Thoning, K. W., and Kahl, J. D. W.: An interpretation of trace gas correlations during Barrow, Alaska, winter dark periods, 1986–1997, J. Geophys. Res., 105, 17267–17278, doi:10.1029/2000JD900167, 2000.

Hegarty, J., Mao, H., and Talbot, R.: Synoptic influences on springtime tropospheric O_3 and CO over the North American export region observed by TES, Atmos. Chem. Phys., 9, 3755–3776, doi:10.5194/acp-9-3755-2009, 2009.

Hegarty, J., Mao, H., and Talbot, R.: Winter- and summertime continental influences on tropospheric O_3 and CO observed by TES over the western North Atlantic Ocean, Atmos. Chem. Phys., 10, 3723–3741, doi:10.5194/acp-10-3723-2010, 2010.

Hirsch, A. I., Munger, J. W., Jacob, D. J., Horowitz, L. W., and Goldstein, A. H.: Seasonal variation of the ozone production efficiency per unit NO_x at Harvard Forest, Massachusetts, J. Geophys. Res., 101, 12659–12666, doi:10.1029/96JD00557, 1996.

ACPD
13, 8901–8937, 2013

Honrath, R. E., Owen, R. C., Val Martin, M., Reid, J. S., Lapina, K., Fialho, P., Dziobak, M. P, Kleissl, J., and Westphal, D. L.: Regional and hemispheric impacts of anthropogenic and biomass burning emissions on summertime CO and O_3 in the North Atlantic lower free troposphere, J. Geophys. Res., 109, D24310, doi:10.1029/2004JD005147, 2004.

Hudman, R. C., Jacob, D. J., Cooper, O. R., Evans, M. J., Heald, C. L., Park. R. J., Fehsenfeld, F., Flocke, F., Holloway, J., Hubler, G., Kita, K., Koike, M., Kondo, Y., Neuman, A., Nowak, J., Oltmans, S., Parrish, D., Roberts, J. M., and Ryerson, T.: Ozone production in transpacific Asian pollution plumes and implications for ozone air quality in California, J. Geophys. Res., 109, D23S10, doi:10.1029/2004JD004974, 2004.

Hudman, R. C., Jacob, D. J., Turquety, S., Leibensperger, E. M., Murray, L. T., Wu, S., Gilliland, A. B., Avery, M., Bertram, T. H., Brune, W., Cohen, R. C., Dibb, J. E., Flocke, F. M., Fried, A., Holloway, J., Neuman, J. A., Orville, R., Perring, A., Ren, X., Sachse, G. W., Singh, H. B., Swanson, A., and Wooldridge, P. J.: Surface and lightning sources of nitrogen oxides over the United States: magnitudes, chemical evolution, and outflow, J. Geophys. Res., 112, D12S05, doi:10.1029/2006JD007912, 2007.

Hudman, R. C., Murray, L. T., Jacob, D. J., Millet, D. B., Turquety, S., Wu, S., Blake, D. R., Goldstein, A. H., Holloway, J., and Sachse, G. W.: Biogenic versus anthropogenic sources of CO in the United States, Geophys. Res. Lett., 35, L04801, doi:10.1029/2007GL032392, 2008.

Hudman, R. C., Murray, L. T., Jacob, D. J., Turquety, S., Wu, S., Millet, D. B., Avery, M., Goldstein, A. H., and Holloway, J.: North American influence on tropospheric ozone and the effects of recent emission reductions: constraints from ICARTT observations, J. Geophys. Res., 114, D07302, doi:10.1029/2008JD010126, 2009.

Isobe, T., Feigelson, E. D., Akritas, M. G., and Babu, G. J.: Linear regression in astronomy, Astrophys. J., 364, 104–113, doi:10.1086/169390, 1990.

Jacob, D. J., Heikes, B. G., Fan, S.-M., Logan, J. A., Mauzerall, D. L., Bradshaw, J. D., Singh, H. B., Gregory, G. L., Talbot, R. W., Blake, D. W., and Sachse, G. W.: Origin of ozone and NO_x in the tropical troposphere: a photochemical analysis of aircraft observations over the South Atlantic basin, J. Geophys. Res., 101, 24235–24250, doi:10.1029/96JD00336, 1996.

Jaffe, D. A. and Wigder, N. L.: Ozone production from wildfires: a critical review, Atmos. Environ., 51, 1–10, doi:10.1016/j.atmosenv.2011.11.062, 2012.

ACPD
13, 8901–8937, 2013

Jourdain, L., Worden, H. M., Worden, J. R., Bowman, K., Li, Q., Eldering, A., Kulawik, S. S., Osterman, G., Boersma, K. F., Fisher, B., Rinsland, C. P., Beer, R., and Gunson, M.: Tropospheric vertical distribution of tropical Atlantic ozone observed by TES during the north African biomass burning season, Geophys. Res. Lett., 34, L04810, doi:10.1029/2006GL028284, 2007.

Kopacz, M., Jacob, D. J., Fisher, J. A., Logan, J. A., Zhang, L., Megretskaia, I. A., Yantosca, R. M., Singh, K., Henze, D. K., Burrows, J. P., Buchwitz, M., Khlystova, I., McMillan, W. W., Gille, J. C., Edwards, D. P., Eldering, A., Thouret, V., and Nedelec, P.: Global estimates of CO sources with high resolution by adjoint inversion of multiple satellite datasets (MOPITT, AIRS, SCIAMACHY, TES), Atmos. Chem. Phys., 10, 855–876, doi:10.5194/acp-10-855-2010, 2010.

Kuhns, H., Green, M., and Etyemezian, V.: Big Bend Regional Aerosol and Visibility Observational (BRAVO) Study Emissions Inventory, Report prepared for BRAVO Steering Committee, Desert Research Institute, Las Vegas, Nevada, 2003.

Labrador, L. J., von Kuhlmann, R., and Lawrence, M. G.: Strong sensitivity of the global mean OH concentration and the tropospheric oxidizing efficiency to the source of NO_x from lightning, Geophys. Res. Lett., 31, L06102, doi:10.1029/2003GL019229, 2004.

Levelt, P. F., van den Oord, G. H. J., Dobber, M. R., Malkki, A., Visser, H., de Vries, J., Stammes, P., Lundell, J. O. V., and Saari, H.: The Ozone Monitoring Instrument, IEEE T. Geosci. Remote, 44, 1093–1101, doi:10.1109/TGRS.2006.872333, 2006.

Liang, Q., Jaegle, L., Hudman, R. C., Turquety, S., Jacob, D. J., Avery, M. A., Browell, E. V., Sachse, G. W., Blake, D. R., Brune, W., Ren, X., Cohen, R. C., Dibb, J. E., Fried, A., Fuelberg, H., Porter, M., Heikes, B. G., Huey, G., Singh, H. B., and Wennberg, P. O.: Summertime influence of Asian pollution in the free troposphere over North America, J. Geophys. Res., 112, D12S11, doi:10.1029/2006JD007919, 2007.

Liu, J., Logan, J. A., Jones, D. B. A., Livesey, N. J., Megretskaia, I., Carouge, C., and Nedelec, P.: Analysis of CO in the tropical troposphere using Aura satellite data and the GEOS-Chem model: insights into transport characteristics of the GEOS meteorological products, Atmos. Chem. Phys., 10, 12207–12232, doi:10.5194/acp-10-12207-2010, 2010.

Liu, X., Bhartia, P. K., Chance, K., Spurr, R. J. D., and Kurosu, T. P.: Ozone profile retrievals from the Ozone Monitoring Instrument, Atmos. Chem. Phys., 10, 2521–2537, doi:10.5194/acp-10-2521-2010, 2010.

ACPD
13, 8901–8937, 2013

Mao, H. and Talbot, R.: O_3 and CO relationships in New England: temporal variations and relationships, J. Geophys. Res., 109, D21304, doi:10.1029/2004JD004913, 2004.
Mao, J., Fan, S., Jacob, D. J., and Travis, K. R.: Radical loss in the atmosphere from Cu–Fe redox coupling in aerosols, Atmos. Chem. Phys., 13, 509–519, doi:10.5194/acp-13-509-2013, 2013.
Martin, R. V., Jacob, D. J., Logan, J. A., Bey, I., Yantosca, R. M., Staudt, A. M., Li, Q., Fiore, A. M., Duncan, B. N., Liu, H., Ginoux, P., and Thouret, V.: Interpretation of TOMS observations of tropical tropospheric ozone with a global model and in situ observations, J. Geophys. Res., 107, 4351, doi:10.1029/2001JD001480, 2002.
Martin, R. V., Sauvage, B., Folkins, I., Sioris, C. E., Boone, C., Bernath, P., and Ziemke, J.: Space-based constraints on the production of nitric oxide by lightning, J. Geophys. Res., 112, D09309, doi:10.1029/2006JD007831, 2007.
Mauzerall, D. L., Logan, J. A., Jacob, D. J., Anderson, B. E., Blake, D. R., Bradshaw, J. D., Heikes, B., Sachse, G. W., Singh, H. B., and Talbot, R. W.: Photochemistry in biomass burning plumes and implications for tropospheric ozone over the tropical south Atlantic, J. Geophys. Res., 103, 8401–8424, doi:10.1029/97JD02612, 1998.
McLinden, C. A., Olsen, S. C., Hannegan, B., Wild, O., Prather, M. J., and Sundet, J.: Stratospheric ozone in 3-D models: a simple chemistry and cross-tropopause flux, J. Geophys. Res., 105, 14653–14666, doi:10.1029/2000JD900124, 2000.
McMillan, W. W., Evans, K. D., Barnet, C. D., Maddy, E., Sachse, G. W., and Disken, G. S.: Validating the AIRS Version 5 CO retrieval with DACOM in situ measurements during INTEX-A and -B, IEEE T. Geosci. Remote, 49, 2802–2813, doi:10.1109/TGRS.2011.2106505, 2011.
McPeters, R. D., Labow, G. J., and Logan, J. A.: Ozone climatological profiles for satellite retrieval algorithms, J. Geophys. Res., 112, D05308, doi:10.1029/2005JD006823, 2007.
Monks, P. S.: A review of the observations and origins of the spring ozone maximum, Atmos. Environ., 34, 3545–3561, doi:10.1016/S1352-2310(00)00129-1, 2000.
Murray, L. T., Jacob, D. J., Logan, J. A., Hudman, R. C., and Koshak, W. J.: Optimized regional and interannual variability of lightning in a global chemical transport constrained by LIS/OTD satellite data, J. Geophys. Res., 117, D20307, doi:10.1029/2012JD017934, 2012.
Nowak, J. B., Parrish, D. D., Neuman, J. A., Holloway, J. S., Cooper, O. R., Ryerson, T. B., Nicks Jr., D. K., Flocke, F., Roberts, J. M., Atlas, E., de Gouw, J. A., Donnelly, S., Dunlea, E., Hubler, G., Huey, L. G., Schauffler, S., Tanner, D. J., Warneke, C., and Fehsenfeld, F. C.: Gas-

ACPD
13, 8901–8937, 2013

phase chemical characteristics of Asian emission plumes observed during ITCT 2K2 over the eastern North Pacific Ocean, J. Geophys. Res., 109, D23S19, doi:10.1029/2003JD004488, 2004.

Olivier, J. G. J. and Berdowski, J. J. M.: Global emissions sources and sinks, in: The Climate System, edited by: Berdowski, J., Guicherit, R., and Heij, B. J., A. A. Balkema Publisher/Swets and Zeitlinger Publishers, Lisse, the Netherlands, 33–78, 2001.

Parazoo, N. C., Denning, A. S., Kawa, S. R., Pawson, S., and Lokupitiya, R.: CO_2 flux estimation errors associated with moist atmospheric processes, Atmos. Chem. Phys., 12, 6405–6416, doi:10.5194/acp-12-6405-2012, 2012.

Park, R. J., Jacob, D. J., Field, B. D., Yantosca, R. M., and Chin, M.: Natural and transboundary pollution influences on sulfate-nitrate-ammonium aerosols in the United States: implications for policy, J. Geophys. Res., 109, D15204, doi:10.1029/2003JD004473, 2004.

Parrish, D. D., Holloway, J. S., Trainer, M., Murphy, P. C., Forbes, F. L., and Fehsenfeld, F. C.: Export of North American pollution ozone to the North Atlantic Ocean, Science, 259, 1436–1439, doi:10.1126/science.259.5100.1436, 1993.

Parrish, D. D., Trainer, M., Holloway, J. S., Lee, J. E., Warshawsky, M. S., Fehsenfeld, F. C., Forbes, G. L., and Moody, J. L.: Export of North American ozone pollution to the North Atlantic Ocean, J. Geophys. Res., 103, 13357–13376, doi:10.1029/98JD00376, 1998.

Price, H. U., Jaffe, D. A., Cooper, O. R., and Doskey, P. V.: Photochemistry, ozone production, and dilution during long-range transport episodes from Eurasia to the northwest United States, J. Geophys. Res., 109, D23S13, doi:10.1029/2003JD004400, 2004.

Rodgers, C. D.: Inverse Method for Atmospheric Sounding: Theory and Practice, World Sci., Hackensack, NJ, 2000.

Sauvage, B., Martin, R. V., van Donkelaar, A., and Ziemke, J. R.: Quantification of the factors controlling tropical tropospheric ozone and the South Atlantic maximum, J. Geophys. Res., 112, D11309, doi:10.1029/2006JD008008, 2007.

Schneider, H. R., Jones, D. B. A., Shi, G. Y., and McElroy, M. B.: Analysis of residual mean transport in the stratosphere, 1. Model description and comparison with satellite data, J. Geophys. Res., 105, 19991–20011, doi:10.1029/2000JD900213, 2000.

Spurr, R. J. D.: VLIDORT: a linearized pseudo-spherical vector discrete ordinate radiative transfer code for forward model and retrieval studies in multilayer scattering media, J. Quant. Spectrosc. Ra., 102, 316–342, 2006.

ACPD
13, 8901–8937, 2013

Stevenson, D. S., Dentener, F. J., Schultz, M. G., Ellingsen, K., van Noije, T. P. C., Wild, O., Zeng, G., Amann, M., Atherton, C. S., Bell, N., Bergmann, D. J., Bey, I., Butler, T., Cofala, J., Collins, W. J., Derwent, R. G., Doherty, R. M., Drevet, J., Eskes, H. J., Fiore, A. M., Gauss, M., Hauglustaine, D. A., Horowitz, L. W., Isaksen, I. S. A., Krol, M. C., Lamarque, J.-F., Lawrence, M. G., Montanaro, V., Muller, J.-F., Pitari, G., Prather, M. J., Pyle, J. A., Rast, S., Rodriguez, J. M., Sanderson, M. G., Savage, N. H., Shindell, D. T., Strahan, S. E., Sudo, K., and Szopa, S.: Multimodel ensemble simulations of present-day and near-future tropospheric ozone, J. Geophys. Res., 111, D08301, doi:10.1029/2005JD006338, 2006.

Susskind, J., Barnet, C. D., Blaisdell, J. M., Center, G. S. F., and Greenbelt, M. D.: Retrieval of atmospheric and surface parameters from AIRS/AMSU/HSB data in the presence of clouds, IEEE T. Geosci. Remote, 41, 390–409, doi:10.1109/TGRS.2002.808236, 2003.

Terao, Y., Logan, J. A., Douglass, A. R., and Stolarski R. S.: Contribution of stratospheric ozone to the interannual variability of tropospheric ozone in the northern extratropics, J. Geophys. Res., 113, D18309, doi:10.1029/2008JD009854, 2008.

Thompson, A. M., Pickering, K. E., McNamara, D. P., Schoeberl, M. R., Hudson, R. D., Kim, J. H., Browell, E. V., Kirchoff, V. W. J. H., and Nganga, D.: Where did tropospheric ozone over southern Africa and the tropical Atlantic come from in October 1992? Insights from TOMS, GTE TRACE A, and SAFARI 1992, J. Geophys. Res., 101, 24251–24278, doi:10.1029/96JD01463, 1996.

Thompson, A. M., Doddridge, B. G., Witte, J. C., Hudson, R. D., Luke, W. T., Johnson, J. E., Johnson, B. J., Oltmans, S. J., and Weiler, R.: A tropical Atlantic paradox: shipboard and satellite views of a tropospheric ozone maximum and wave-one in January–February 1999, Geophys. Res. Lett., 27, 3317–3320, doi:10.1029/1999GL011273, 2000.

van der Werf, G. R., Randerson, J. T., Giglio, L., Collatz, G. J., Mu, M., Kasibhatla, P. S., Morton, D. C., DeFries, R. S., Jin, Y., and van Leeuwen, T. T.: Global fire emissions and the contribution of deforestation, savanna, forest, agricultural, and peat fires (1997–2009), Atmos. Chem. Phys., 10, 11707–11735, doi:10.5194/acp-10-11707-2010, 2010.

van het Bolscher, M., Pereira, J., Spessa, A., Dalsoren, S., van Nojie, T., and Szopa, S.: Reanalysis of the tropospheric chemical composition over the past 40 yr: a long-term global modeling study of tropospheric chemistry funded under the 5th EU framework programme, edited by: Schultz, M. and Rast, S., Rep. EVK2-CT-2002-00170, Max Planck Inst. for Meteorol., Hamburg, Germany, 1–77, 2008.

ACPD
13, 8901–8937, 2013

Vestreng, V. and Klein, H.: Emission data reported to UN-ECE/EMEP, Quality assurance and trend analysis and Presentation of WebDab, MSC-W Status Report 2002, Norwegian Meteorological Institute, Oslo, Norway, 2002.

Voulgarakis, A., Telford, P. J., Aghedo, A. M., Braesicke, P., Faluvegi, G., Abraham, N. L., Bowman, K. W., Pyle, J. A., and Shindell, D. T.: Global multi-year O_3–CO correlation patterns from models and TES satellite observations, Atmos. Chem. Phys., 11, 5819–5838, doi:10.5194/acp-11-5819-2011, 2011.

Warner, J., Comer, M. M., Barnet, C. D., McMillan, W. W., Wolf, W., Maddy, E., and Sachse, G.: A comparison of satellite tropospheric carbon monoxide measurements from AIRS and MOPITT during INTEX-A, J. Geophys, Res., 112, D12S17, doi:10.1029/2006JD007925, 2007.

Warner, J. X., Wei, Z., Strow, L. L., Barnet, C. D., Sparling, L. C., Diskin, G., and Sachse, G.: Improved agreement of AIRS tropospheric carbon monoxide products with other EOS sensors using optimal estimation retrievals, Atmos. Chem. Phys., 10, 9521–9533, doi:10.5194/acp-10-9521-2010, 2010.

Waugh, D. W. and Polvani, L. M.: Climatology of intrusions into the tropical upper troposphere, Geophys. Res. Lett., 27, 3857–3860, doi:10.1029/2000GL012250, 2000.

Wild, O.: Modelling the global tropospheric ozone budget: exploring the variability in current models, Atmos. Chem. Phys., 7, 2643–2660, doi:10.5194/acp-7-2643-2007, 2007.

Wu, S., Mickley, L. J., Jacob, D. J., Logan, J. A., Yantosca, R. M., and Rind, D.: Why are there large differences between models in global budgets of tropospheric ozone?, J. Geophys. Res., 112, D05302, doi:10.1029/2006JD007801, 2007.

Yevich, R. and Logan, J. A.: An assesment of biofuel use and burning of agricultural waste in the developing world, Global Biogeochem. Cy., 17, 1095, doi:10.1029/2002GB001952, 2003.

Yurganov, L. N., McMillan, W. W., Dzhola, A. V., Grechko, E. I., Johnes, N. B., and van der Werf, G. R.: Global AIRS and MOPITT CO measurements: validation, comparison, and links to biomass burning variations and carbon cycle, J. Geophys. Res., 113, D09301, doi:10.1029/2007JD009229, 2008.

Yurganov, L., McMillan, W., Grechko, E., and Dzhola, A.: Analysis of global and regional CO burdens measured from space between 2000 and 2009 and validated by ground-based solar tracking spectrometers, Atmos. Chem. Phys., 10, 3479–3494, doi:10.5194/acp-10-3479-2010, 2010.

Zahn, A., Brenninkmeijer, C. A. M., Asman, W. A. H., Crutzen, P. J., Heinrich, G., Fischer, H., Cuijpers, J. W. M., and van Velthoven, P. F. J.: Budgets of O_3 and CO in the upper tro-

ACPD
13, 8901–8937, 2013

posphere: CARIBIC passenger aircraft results 1997–2001, J. Geophys. Res., 107, 4337, doi:10.1029/2001JD001529, 2002.

Zhang, L., Jacob, D. J., Bowman, K. W., Logan, J. A., Turquety, S., Hudman, R. C., Li, Q., Beer, R., Worden, H. M., Worden, J. R., Rinsland, C. P., Kulawik, S. S., Lampel, M. C., Shephard, M. W., Fisher, B. M., Eldering, A., and Avery, M. A.: Ozone–CO correlations determined by the TES satellite instrument in continental outflow regions, Geophys. Res. Lett., 33, L18804, doi:10.1029/2006GL026399, 2006.

Zhang, L., Jacob, D. J., Boersma, K. F., Jaffe, D. A., Olson, J. R., Bowman, K. W., Worden, J. R., Thompson, A. M., Avery, M. A., Cohen, R. C., Dibb, J. E., Flock, F. M., Fuelberg, H. E., Huey, L. G., McMillan, W. W., Singh, H. B., and Weinheimer, A. J.: Transpacific transport of ozone pollution and the effect of recent Asian emission increases on air quality in North America: an integrated analysis using satellite, aircraft, ozonesonde, and surface observations, Atmos. Chem. Phys., 8, 6117–6136, doi:10.5194/acp-8-6117-2008, 2008.

Zhang, L., Jacob, D. J., Liu, X., Logan, J. A., Chance, K., Eldering, A., and Bojkov, B. R.: Intercomparison methods for satellite measurements of atmospheric composition: application to tropospheric ozone from TES and OMI, Atmos. Chem. Phys., 10, 4725–4739, doi:10.5194/acp-10-4725-2010, 2010.

Zhang, Q., Streets, D. G., Carmichael, G. R., He, K. B., Huo, H., Kannari, A., Klimont, Z., Park, I. S., Reddy, S., Fu, J. S., Chen, D., Duan, L., Lei, Y., Wang, L. T., and Yao, Z. L.: Asian emissions in 2006 for the NASA INTEX-B mission, Atmos. Chem. Phys., 9, 5131–5153, doi:10.5194/acp-9-5131-2009, 2009.

ACPD
13, 8901–8937, 2013

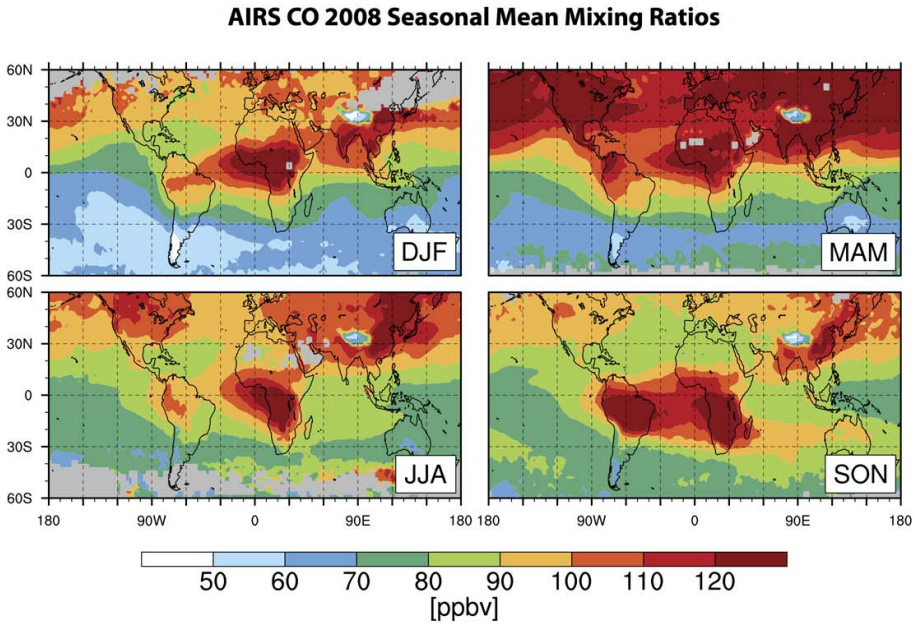

Fig. 1a. Seasonal mean AIRS CO mixing ratios at 700–400 hPa for 2008. Data are plotted on the 2° × 2.5° GEOS-Chem grid. Gray indicates insufficient data (see text).

ACPD
13, 8901–8937, 2013

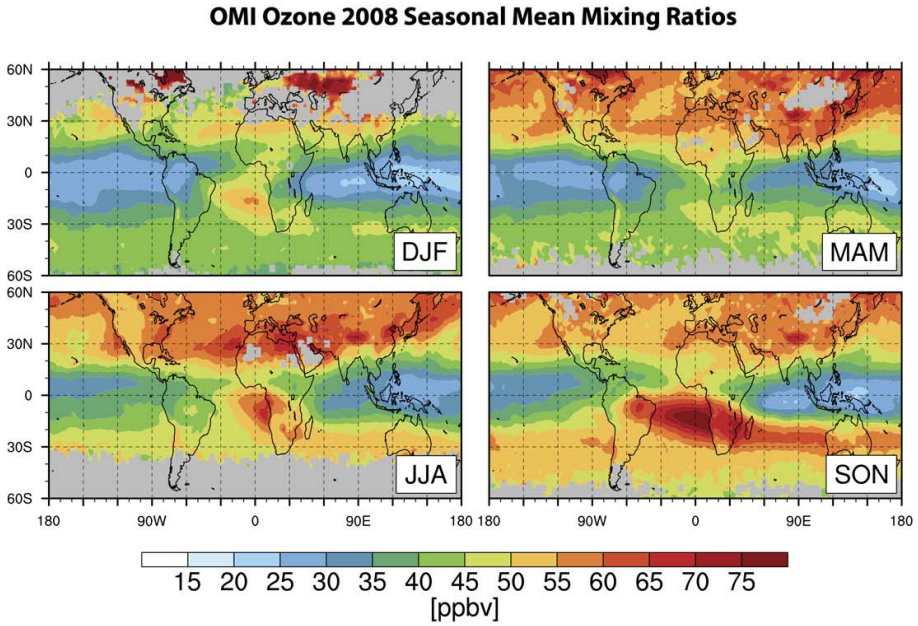

Fig. 1b. Same as Fig. 1a but for OMI ozone mixing ratios at 700–400 hPa.

ACPD
13, 8901–8937, 2013

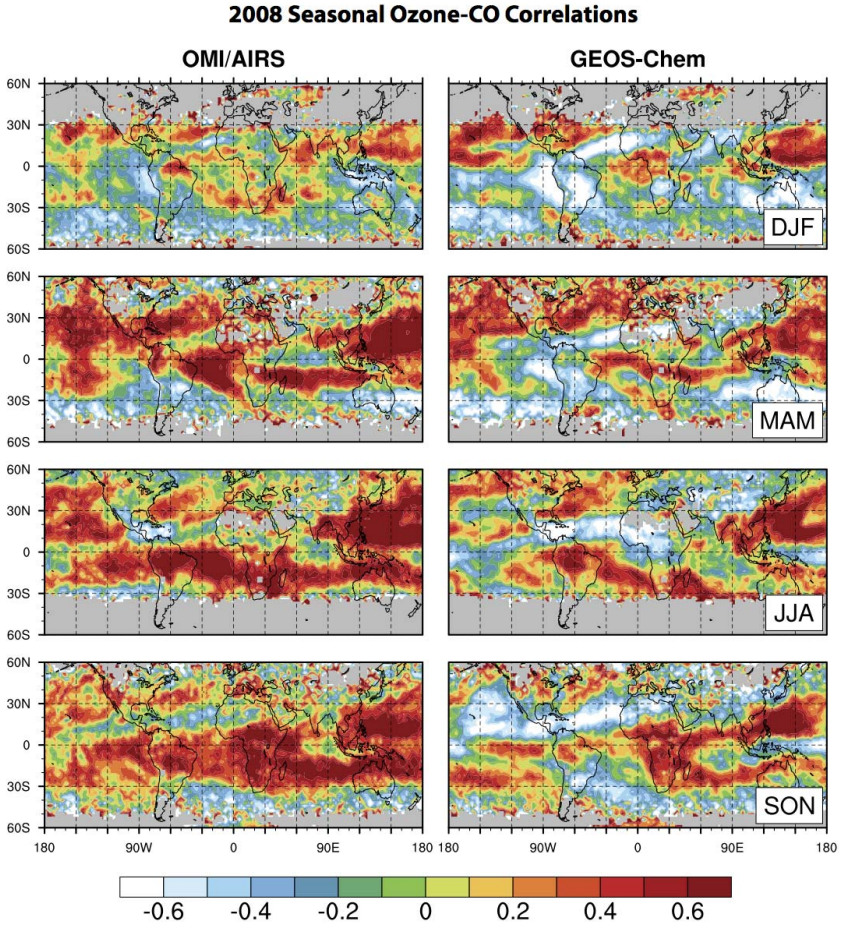

Fig. 2a. Ozone–CO correlation coefficients (r) for OMI/AIRS and GEOS-Chem for each season of 2008. The correlation coefficients are computed from daily data on the 2° × 2.5° GEOS-Chem grid. Gray indicates insufficient data.

ACPD
13, 8901–8937, 2013

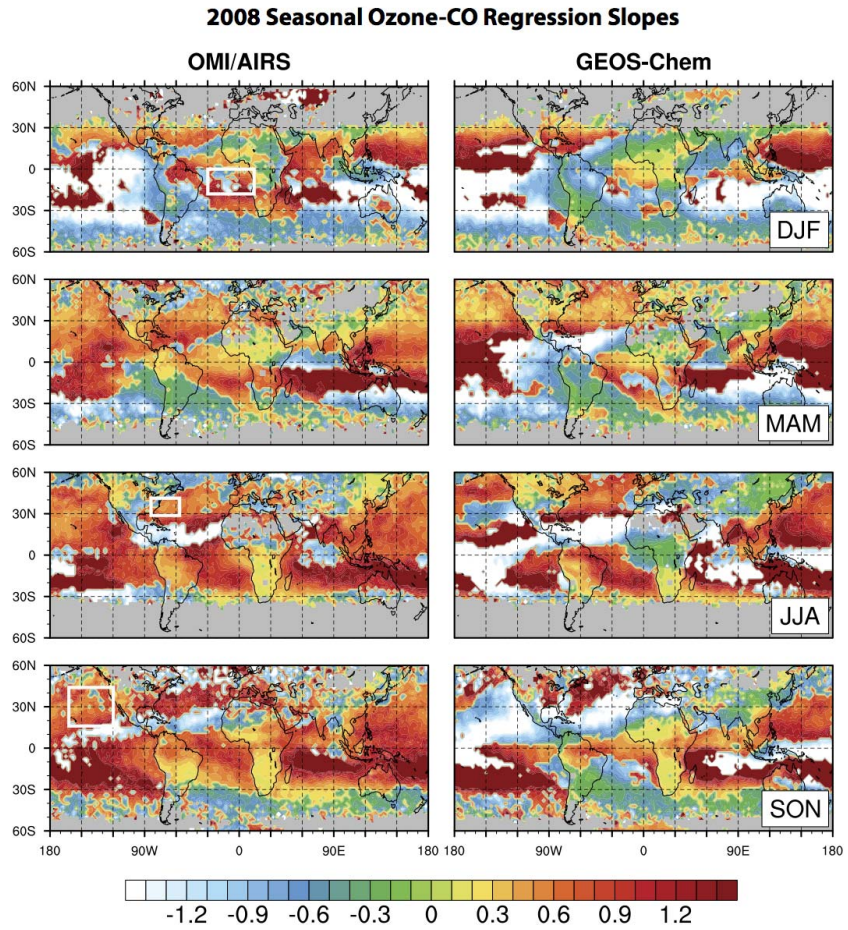

Fig. 2b. Same as Fig. 2a but for the ozone–CO reduced-major-axis regression slope (dO_3/dCO). White boxes mark regions analyzed further in Sect. 4.2 and Fig. 5.

ACPD
13, 8901–8937, 2013

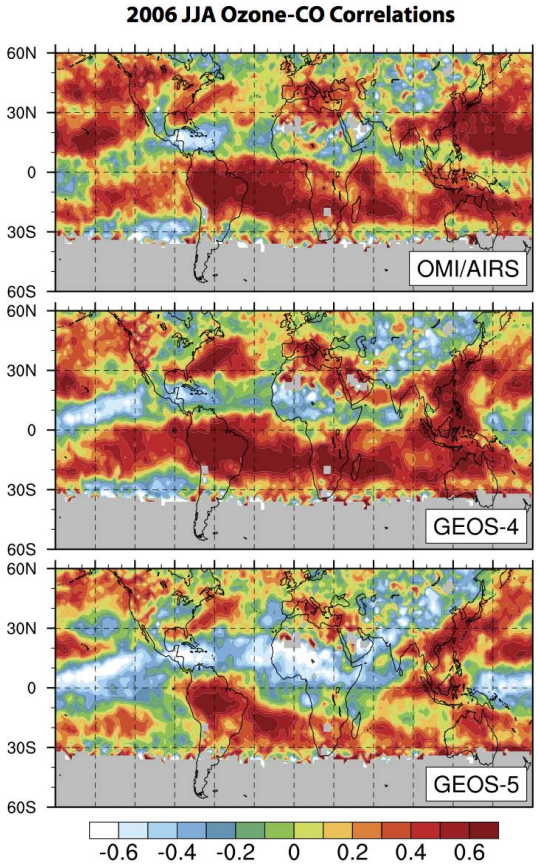

Fig. 3. Ozone–CO correlation coefficients (r) for JJA 2006 from OMI/AIRS and from GEOS-Chem driven by GEOS-4 and GEOS-5 meteorology. Gray indicates insufficient data.

ACPD
13, 8901–8937, 2013

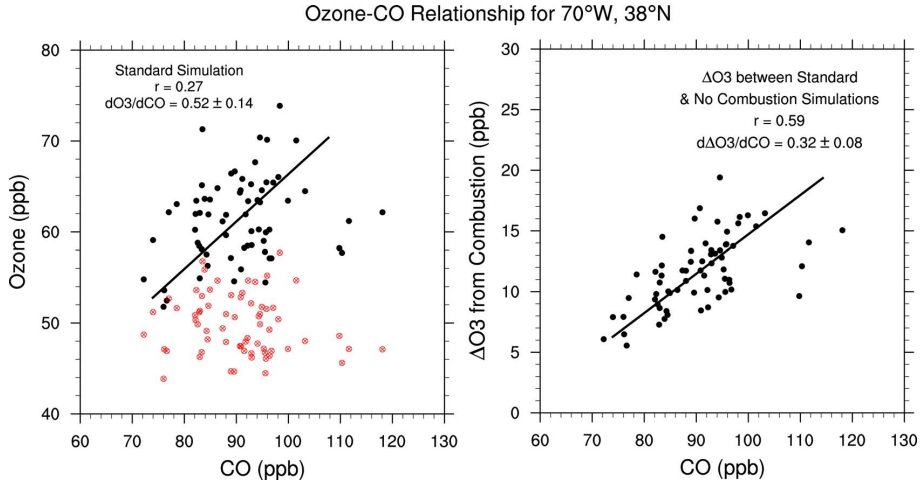

Fig. 4. Ozone–CO relationships at 700–400 hPa in JJA 2008 over the western North Atlantic ($2^{\circ} \times 2.5^{\circ}$ grid square centered at 38° N, 70° W). Values are GEOS-Chem model results sampled daily at the local OMI and AIRS satellite overpass times and weighted by the vertical sensitivity of the instruments. In the left panel, ozone concentrations in black are from the standard simulation and in red for the sensitivity simulation including no combustion sources. CO concentrations are from the standard simulation in both cases. The right panel shows the ozone difference ΔO_3 between the standard and sensitivity simulations as a function of CO from the standard simulation, with slope $d\Delta O_3/dCO$. All regression lines are obtained by the reduced-major-axis (RMA) method and the slope bound is the 95 % confidence interval calculated from nonparametric bootstrapping.

ACPD
13, 8901–8937, 2013

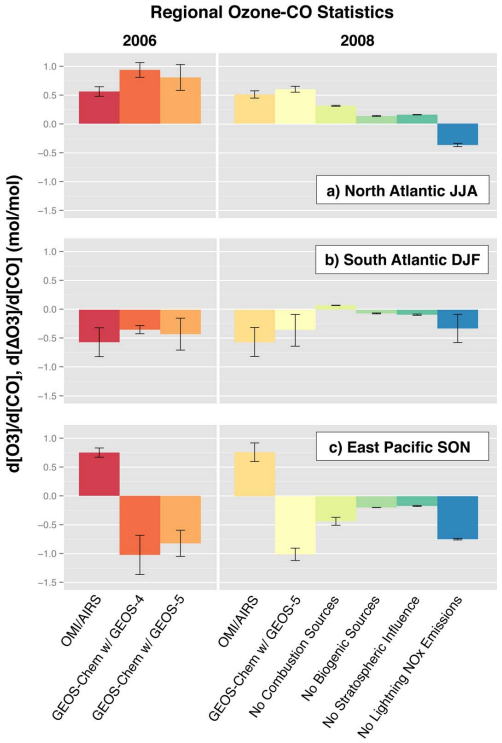

Fig. 5. Regional bar plots of ozone–CO statistics for **(a)** the western North Atlantic (30°–40° N, 60°–80° W) in JJA; **(b)** the South Atlantic (0°–20° S, 30° W–10° E) in DJF; and **(c)** the East Pacific (20°–40° N, 120°–160° W) in SON. Region boundaries are shown in white in Fig. 2b. From left to right, the bars show dO_3/dCO for OMI/AIRS, GEOS-Chem driven by GEOS-4, and GEOS-Chem driven by GEOS-5 in 2006; dO_3/dCO for OMI/AIRS and GEOS-Chem driven by GEOS-5 in 2008; and $d\Delta O_3/dCO$ for simulations without combustion sources, biogenic sources, stratospheric influence, and lightning NO_x emissions for 2008. See text for explanation of slope bounds.

ACPD
13, 8901–8937, 2013